Condensate Formation in a Dark State of a Driven Atom-Cavity System

Jim Skulte,[1,2,*] Phatthamon Kongkhambut,[1,*] Sahana Rao,[1] Ludwig Mathey,[1,2] Hans Keßler,[1] Andreas Hemmerich,[1,2] and Jayson G. Cosme[3]

[1]*Zentrum für Optische Quantentechnologien and Institut für Laser-Physik, Universität Hamburg, 22761 Hamburg, Germany*
[2]*The Hamburg Center for Ultrafast Imaging, Luruper Chaussee 149, 22761 Hamburg, Germany*
[3]*National Institute of Physics, University of the Philippines, Diliman, Quezon City 1101, Philippines*

(Received 6 September 2022; accepted 14 March 2023; published 21 April 2023)

We demonstrate the formation of a condensate in a dark state of momentum states, in a pumped and shaken cavity-BEC system. The system consists of an ultracold quantum gas in a high-finesse cavity, which is pumped transversely by a phase-modulated laser. This phase-modulated pumping couples the atomic ground state to a superposition of excited momentum states, which decouples from the cavity field. We demonstrate how to achieve condensation in this state, supported by time-of-flight and photon emission measurements. With this, we show that the dark state concept provides a general approach to efficiently prepare complex many-body states in an open quantum system.

DOI: 10.1103/PhysRevLett.130.163603

While dissipation is in general perceived as a destructive feature of a quantum system, it can also be utilized to engineer nontrivial states, often in conjunction with driving a system out of equilibrium. A prominent experimental platform for this purpose is ultracold quantum gases coupled to high-finesse optical cavities [1–4], due to the well-controlled dissipative channel resulting from the photon emission out of the cavity. Paradigmatic models of light-matter interaction can be explored, such as the celebrated Dicke model that describes the interaction between N two-level atoms with a single quantized light mode [5]. The driven-dissipative Dicke model, an extension of the standard Dicke model, captures the scenario, when both external driving and dissipation are present [6,7]. A wealth of phases, unique to driven light-matter systems, have been proposed and realized using variations of driven Dicke models, such as the three-level Dicke model [8–20]. In particular, the dissipation channel of the cavity has been utilized to demonstrate the emergence of nonequilibrium or dynamical phases [19,21–35].

An intriguing class of quantum states in light-matter systems, well known in quantum optics, are the so-called dark states [36]. These are superpositions of matter states with relative phases such that the quantum mechanical amplitudes, coupling the different sectors to an irradiated light field, interfere destructively. As a consequence, dark states decouple from the light field. Dark states play a crucial role in physical phenomena, such as stimulated Raman adiabatic passage [37,38], electromagnetically induced transparency [39,40], lasing without inversion [41,42], and combinations of these topics [9,20,43,44]. In conventional quantum optics scenarios, dark states typically arise on a single-particle level. In this Letter, we use the dark state concept in a many-body context, specifically condensation. Our study suggests how the concept of dark state formation can be utilized in the context of quantum state engineering via dissipation.

In this Letter, we demonstrate in theory and experiment a robust condensate formation in a dark state of a driven atom-cavity system, approximately described by a parametrically driven three-level open Dicke model introduced in Refs. [17,19]. We consider a Bose-Einstein condensate (BEC) prepared in a high-finesse cavity, which is transversely pumped with a shaken one-dimensional optical lattice, as sketched in Fig. 1(a). Previously, we explored the weakly resonantly driven scenario leading to an incommensurate time crystal (ITC) [17,19,26]. Here, technical improvements in our setup allowed us to study theoretically and experimentally the so far unexplored regime of strong driving and a wider range of driving frequencies, which reveals that the ITC has transient character in certain parameter regimes, such that the atoms relax into a dark state of the atom-cavity system eventually.

To understand the dark state and to identify the relevant driving parameters, we employ the time-dependent atom-cavity Hamiltonian in Refs. [17,45] and an approximative parametrically driven three-level Dicke model [17,19], which includes only three atomic modes denoted as $|N\rangle$, $|B\rangle$, and $|D\rangle$, in a plane-wave expansion of the atomic field operator. These modes are illustrated in terms of their momentum components in Fig. 1(b) and form the V-shaped three-level system sketched in Fig. 1(c). The normal state $|N\rangle \equiv |(0,0)\hbar k\rangle$ corresponds to a homogeneous density in real space, wherein all atoms occupy the lowest momentum mode $\{p_y, p_z\} = \{0,0\}\hbar k$ (k is the wave number of the pump field). The pump leads to a light shift of $-\epsilon_p \omega_{\mathrm{rec}}/2$, where ϵ_p is the unitless pump intensity and ω_{rec} is the atomic

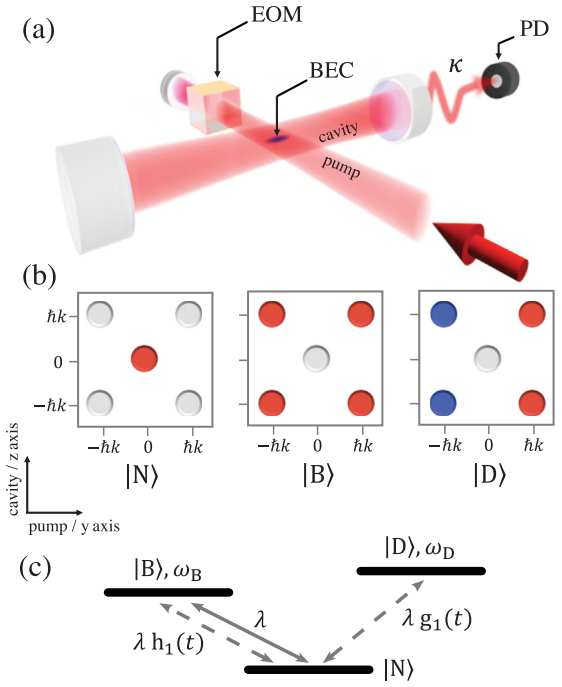

FIG. 1. (a) Sketch of the experimental setup. An electro-optical modulator (EOM) is used to modulate the phase of the pump field, which results in shaking the pump potential. The light leaking out the cavity is detected using a photo diode (PD). (b) Sketch of the momentum distribution of the three relevant superpositions of momentum modes, the normal state $|N\rangle$, the bright state $|B\rangle$, and the dark state $|D\rangle$, which form a three-level Dicke model shown in (c) with the atom-cavity coupling λ and the shaking-induced functions $h_1(t)$ and $g_1(t)$. The colors in (b) represent the phase of the momentum states, where blue indicates a phase shift of π relative to red.

recoil frequency. The bright state $|B\rangle \equiv \sum_{\nu,\mu\in\{-1,1\}} |\nu\hbar k, \mu\hbar k\rangle$ is defined as the in-phase superposition of the $\{\pm 1, \pm 1\}\hbar k$ momentum modes as depicted in Fig. 1(b). The real-space wave function of this state is $\propto \cos(ky)\cos(kz)$, which has even parity with respect to the inversion $(y, z) \to (-y, -z)$. It exhibits a kinetic energy of $2E_{\rm rec}$ and is light shifted by the pump wave by $-3\epsilon_p\omega_{\rm rec}/4$ such that its frequency separation relative to $|N\rangle$ is $\omega_B = (2 - \epsilon_p/4)\omega_{\rm rec}$. The dark state $|D\rangle \equiv \sum_{\nu,\mu\in\{-1,1\}} \nu|\nu\hbar k, \mu\hbar k\rangle$ is defined as the out-of-phase superposition of the $\{+1, \pm 1\}\hbar k$ and $\{-1, \pm 1\}\hbar k$ momentum modes. In real space, its order parameter is $\propto \sin(ky)\cos(kz)$, which has odd parity under the inversion $(y, z) \to (-y, -z)$.

The density distributions of the dark state $|D\rangle$ and the bright state $|B\rangle$ both prohibit collective scattering of photons into the cavity. Nonetheless, any admixture of the normal state $|N\rangle$ to the bright state $|B\rangle$ leads to a checkerboard pattern of the atomic density that allows pump photons to scatter into the cavity, which is the reason we refer to $|B\rangle$ as a bright state. Above a critical pump strength, the system forms a superradiant (SR) phase as its stationary state, in which a superposition of $|B\rangle$ and $|N\rangle$ produces a density grating trapped by the intracavity optical lattice composed of the pump and cavity fields. In contrast to $|B\rangle$, the density grating of the dark state $|D\rangle$, due to its odd parity is shifted along the pump direction by a quarter of the pump wavelength, such that the atomic positions coincide with the nodes of the pump lattice, motivating our terminology of bond-density waves in Refs. [17,19]. Hence, even if $|N\rangle$ is admixed to the dark state $|D\rangle$, scattering of pump photons remains suppressed, meaning that for any superposition of the normal and the dark state collective scattering of photons into the cavity cannot occur. The dark state $|D\rangle$ exhibits the same kinetic energy $2E_{\rm rec}$ as $|B\rangle$, while its light shift due to the pump lattice is only $-\epsilon_p\omega_{\rm rec}/4$. Thus, its frequency relative to that of $|N\rangle$ is $\omega_D = (2 + \epsilon_p/4)\omega_{\rm rec}$.

To excite the dark state, we shake the pump lattice by introducing a time-dependent phase in the pump field, $\cos(ky + \phi(t))$, where $\phi(t) = f_0 \sin(\omega_{\rm dr} t)$, f_0 is the driving strength, and $\omega_{\rm dr}$ is the driving frequency. The excitation mechanism is readily understood by means of the three-level Dicke model $\hat{H} = \hat{H}_{\rm stat} + \hat{H}_{\rm dyn}$ with a static part,

$$\hat{H}_{\rm stat}/\hbar = \omega\hat{a}^\dagger\hat{a} + [\omega_B - \Omega(f_0)]\hat{J}_z^B + [\omega_D + \Omega(f_0)]\hat{J}_z^D + \frac{2\lambda}{\sqrt{N_a}}(\hat{a}^\dagger + \hat{a})J_0(f_0)\hat{J}_x^B, \quad (1)$$

and a dynamical part,

$$\hat{H}_{\rm dyn}/\hbar = h_2(t)\Delta\omega_{BD}(\hat{J}_z^D - \hat{J}_z^B) + 2g_2(t)\Delta\omega_{BD}\hat{J}_x^{BD} + \frac{4\lambda}{\sqrt{N_a}}(\hat{a}^\dagger + \hat{a})[h_1(t)\hat{J}_x^B - g_1(t)\hat{J}_x^D], \quad (2)$$

where $\Omega(f_0) = (\epsilon_p\omega_{\rm rec}/4)[1 - J_0(2f_0)]$, $\Delta\omega_{BD} = (\omega_B - \omega_D)$, $h_m(t) = \sum_{n=1}^{\infty} J_{2n}(mf_0)\cos(2n\omega_{\rm dr}t)$, $g_m(t) = \sum_{n=1}^{\infty} J_{2n-1}(mf_0)\sin[(2n-1)\omega_{\rm dr}t]$, and $J_n(r)$ is the nth Bessel function of the first kind. The time-dependent terms introduced by the pump lattice shaking are $h_m(t)$ and $g_m(t)$. Details on the derivation of this Hamiltonian are given in the Supplemental Material [45]. The pseudospin operators $\hat{J}_\mu^B$ ($\mu \in \{x, y, z\}$) describe the coupling to the bright state since $\hat{J}_+^B \equiv \hat{J}_x^B + i\hat{J}_y^B = |B\rangle\langle N|$. Accordingly, $\hat{J}_\mu^D$ is related to the dark state as $\hat{J}_+^D \equiv \hat{J}_x^D + i\hat{J}_y^D = |D\rangle\langle N|$. We see from the last term of Eq. (2) that $|D\rangle$ can be coupled to the cavity mode via the time-dependent shaking of the pump, resulting in a periodic coupling between $|D\rangle$ and $|N\rangle$. Note that the necessary nonzero amplitude $g_1(t)$ can be provided by phase modulation, which breaks the discrete translation symmetry along the pump axis, but not by amplitude modulation. We consider the recoil-resolved regime, i.e., the loss rate of the cavity photons κ is comparable to the recoil frequency $\omega_{\rm rec}$, which for our system is $\omega_{\rm rec} = 2\pi \times 3.6$ kHz. We emphasize the importance of this regime [48,49] to

protect the dark state from detrimental resonant excitations to higher energy momentum states.

Next, we discuss the dynamics of the system by solving the semiclassical equations of motion of the three-level model Eq. (2) and those of the atom-cavity Hamiltonian [45] including fluctuations due to photon emission out of the cavity. For the three-level model, the dark state occupation is $\langle \hat{J}^D \rangle + 1/2$. For the full atom-cavity model, we apply the following protocol: the pump laser strength is linearly increased within 10 ms, such that we always initially prepare the SR phase. After a holding time of 0.5 ms, the phase of the pump lattice is modulated for 7 driving cycles, starting at $t = t_0$. We choose 7 driving cycles since, as is later seen in the experiment, the dark state occupation N_D is found to equilibrate after 6 driving cycles due to heating [45]. Subsequently, we adiabatically ramp-down the pump strength in 0.5 ms and calculate N_D as the sum of the occupations in the $\{\pm 1, \pm 1\}\hbar k$ modes. The ramp-down is necessary to remove all $\{\pm 1, \pm 1\}\hbar k$ populations, associated with $|B\rangle$ rather than $|D\rangle$, by transferring $|B\rangle$ into $|N\rangle$, which does not affect $|D\rangle$. In Fig. 2, we construct the phase diagrams of the three-level and the full models, plotting N_D for different driving parameters. Our previous work on the emergence of an ITC involved the regime around $\omega_{\mathrm{dr}} \in [1, 1.2] \times \omega_D$ and $f_{0,\mathrm{theory}} < 0.4$ [17,19]. We find qualitative agreement between the numerical simulations of the full atom-cavity system and the driven three-level Dicke model as seen in Fig. 2. Significant occupation of the dark state is observed in a large area of the phase diagram for $\omega_{\mathrm{dr}} > \omega_D$ and also in a small area close to the resonance $\omega_{\mathrm{dr}} \approx \omega_D$. We note that the area in the driving parameter space, where the dark state becomes dynamically occupied, is larger in the full atom-cavity model as compared to the three-level Dicke model. This can be attributed to the $\{0, \pm 2\}\hbar k$ and $\{\pm 2, 0\}\hbar k$ modes, which are neglected in the three-level model [45]. Atoms in these modes may be transferred to the dark state upon scattering photons into the cavity, thus increasing its efficient population. This process competes with a direct resonant transfer of atoms into the second band of the pump wave without scattering photons into the cavity, which impedes efficient population of the dark state as detailed in the Supplemental Material [45]. The respective resonance frequency arises in Fig. 2 for $\omega_{\mathrm{dr}}/\omega_D \approx 1.7$, i.e., slightly outside the shown range.

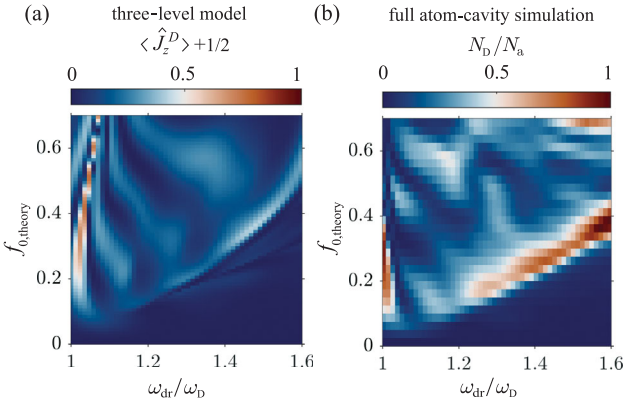

FIG. 2. (a),(b) Population of the dark state for different driving frequencies ω_{dr} and driving strengths $f_{0,\mathrm{theory}}$. The driving frequency axis is rescaled by the characteristic frequency of the dark state ω_D. (a) The results from the three-level model and (b) the full atom-cavity simulation. The phase diagrams are constructed for 7 driving cycles.

Next, we employ the truncated Wigner approximation (TWA) to capture the leading-order quantum effects [26,50–52]. We include not only the dissipation due to photon emission out of the cavity but also the associated fluctuations. We further demonstrate that the observed dark state is indeed a finite momentum condensate by calculating the eigenvalues of the single-particle correlation function at equal time, $\langle \Psi(y,z)^\dagger \Psi(y',z') \rangle$, for our full atom-cavity model. This appears in the Penrose-Onsager criterion for condensates, and its largest eigenvalue corresponds to the condensate fraction [53]. We denote the eigenvalues as n_{NO}. We show in Fig. 3(a) the n_{NO} obtained from TWA simulations for the same pump protocol used in Fig. 2(b), but without the final ramp-down of the pump wave. When the system enters the SR phase (at about 5.2 ms), the condensate fragments manifested in the

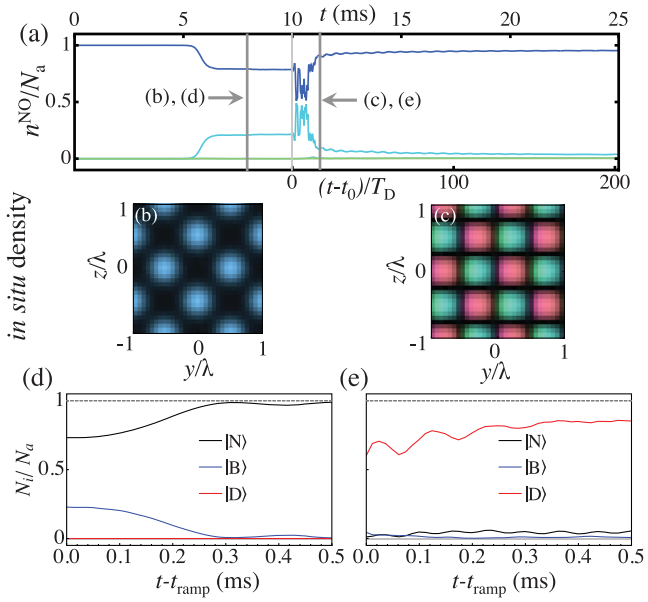

FIG. 3. (a) Simulations of the evolution of the three highest eigenvalues of the single-particle correlation function are shown. Gray dashed and solid vertical lines denote, respectively, the times when the snapshots of the single-particle densities in (b) and (c) are taken. The real-space densities in (b) and (c) are color coded to show the phase of $\Psi(y,z)$. (d),(e) Evolution of the occupations of $|N\rangle$, $|B\rangle$, and $|D\rangle$, while the pump is adiabatically ramped down. Panels (d) and (e), respectively, correspond to initial conditions according to the dashed and solid gray vertical lines in (a).

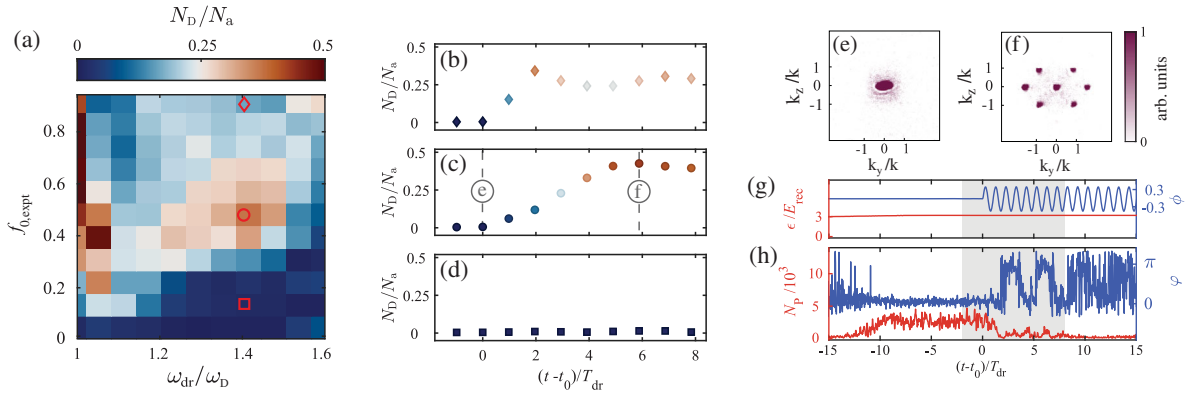

FIG. 4. Experimental phase diagram of the population of the dark state for different driving frequencies ω_{dr} and driving strengths $f_{0,exp}$. The driving frequency axis is rescaled by the characteristic frequency of the dark state ω_D. The phase diagram is constructed for 6 driving cycles. (b)–(d) Population of the dark state as a function of the driving cycles for the parameter sets marked by a diamond, a circle, and a rectangle in (a). The population of the dark state is rescaled by the total particle number N_a for different driving cycles derived from time-of-flight (TOF) images in (b)–(d). Examples of TOF images are provided before shaking starts at $t = 0$ (e) and after around 6 driving cycles (f). All TOF images are obtained after an adiabatic ramp-down of the pump wave and ballistic expansion of 25 ms. (g) Time sequence for the pump strength (red) and the phase ϕ of the pump field (blue). (h) Phase difference φ between the pump and intracavity field (blue) and intracavity photon number N_P (red) for the driving parameters marked by a circle in (a).

reduction of the largest eigenvalue and the corresponding increase of the second largest eigenvalue [54]. The real-space density $|\Psi(y,z)|^2$ shown in Fig. 3(b) illustrates the prevailing SR phase at the time indicated by the dashed gray line, before driving starts at $t = t_0$. In Fig. 3(c), we show $|\Psi(y,z)|^2$ at the time indicated by the solid gray line, after driving has acted for about 0.6 ms, indicating a substantial population of the dark state. The zeros (black regions) coincide with the intensity maxima of the pump lattice along the y direction, while there is no significant standing wave potential along the cavity direction. The different colors in Fig. 3(c) denote opposite phases of $\Psi(y,z)$. In Figs. 3(d) and 3(e), we show the occupations of the relevant states as the pump lattice is ramped down at the times indicated by the dashed [Fig. 3(d)] and solid [Fig. 3(e)] gray lines. It can be seen in Fig. 3(d) that for the SR phase [prevailing at the time denoted by the dashed vertical line in Fig. 3(a)] practically all atoms are transferred back to the normal state $|N\rangle$ after the ramp-down. On the other hand, for the driven case in Fig. 3(e), associated with the time indicated by the solid gray line in Fig. 3(a), the dark state $|D\rangle$ has the largest occupation at $t = t_{ramp}$. After the ramp-down, its occupation increases further, forming a long-lived state, compared to the decay time of the SR state. These results corroborate that the population of the $\{\pm 1, \pm 1\}\hbar k$ modes after the pump is adiabatically switched off is the appropriate observable to quantify the *in situ* occupation of the dark state.

Finally, we experimentally demonstrate driving-induced condensation into a dark state of the atom-cavity system [45]. We present in Fig. 4(a) the resulting experimental phase diagram of the occupation of N_D for varying driving parameters. We find qualitative agreement with the theoretical phase diagrams depicted in Fig. 2. For technical reasons, such as atom losses, a complete population inversion into the dark state, as seen in the numerical simulations, is not observed in the experiment. We note that there is a slight difference between the numerical and the experimental results for the driving strength needed to populate the dark state. This can possibly be attributed to the pump in the experiment having a nonzero width in frequency space, so that the effective pump power is smaller than it would be for monochromatic pump beam. Therefore, the experimental realization might require a nominally larger pump power than in the theoretical model.

Figures 4(b)–4(d) show the occupation of the dark state for varying numbers of driving cycles and fixed driving frequencies. Each panel corresponds to a value of the driving strength $f_{0,exp}$ indicated by the red markers in Fig. 4(a). Between the red circular and the red rectangular marker, there is a sharp transition from large occupation of $|D\rangle$ [see also Fig. 4(c)] toward a region where $|D\rangle$ is practically unoccupied [see also Fig. 4(d)]. In the limit of strong driving around the diamond-shaped marker in Fig. 4(a), the dark state becomes highly occupied after only 2 driving cycles, but the occupation number slightly decreases again for larger numbers of driving cycles as shown in Fig. 4(b). This is explained by the excitation of the $|\pm 2\hbar k, 0\rangle$ modes, as discussed below. Each data point is obtained via averaging over 10 TOF images. We also present the corresponding TOF images [see Figs. 4(e) and 4(f)] at two instances of time, i.e., at $t = t_0$ before driving is started and after six driving cycles at $t = t_0 + 6T_{dr}$ as indicated in Fig. 4(c). These TOF images correspond to the spatial orders calculated in Figs. 3(d) and 3(e). We display the time evolution of the cavity field for a single experimental realization in Fig. 4(h) showcasing the

vanishing intracavity light field as a macroscopic fraction of the atoms occupy the dark state.

For the case depicted in Fig. 4(c), we find that initially N_D increases and saturates beyond 6 driving cycles. The system approaches a steady state because of atom losses before all atoms can be transferred into the dark state. In contrast to the SR phase in Fig. 4(e), the large occupation of the four momentum components $\{\pm 1, \pm 1\}\hbar k$ in Fig. 4(f) in combination with the small intracavity photon number in Fig. 4(h) indicates a large occupation of the dark state $|D\rangle$. Furthermore, a substantial fraction of atoms populates the $\{\pm 2, 0\}\hbar k$ momentum modes as the driving frequency is tuned close to the resonance frequency for excitation to the second band of the pump wave. This process inhibits efficient population of the dark state as is discussed in the Supplemental Material [45]. For reasons explained in Ref. [45], in the experiment, the respective resonance is shifted to $\omega_{\mathrm{dr}}/\omega_D \approx 1.45$, i.e., within the domain shown in Fig. 4(a), acting to suppress the dark state population on the right side of the red circle.

In conclusion, in an atom-cavity system pumped by a periodically shaken standing wave, we have found that in a specific parameter domain, a stationary excited dark state condensate emerges, in which scattering of pump photons into the cavity mode is suppressed. We show that a three-level Dicke model captures this phenomenon qualitatively. Both theoretically and experimentally, we observe that, upon adiabatic ramp-down of the pump wave, the atomic condensate in the dark state is essentially unaffected, while the bright sector of the system undergoes a dynamical phase transition [3]. Our work points out a general approach to form stationary excited many-body states using the concept of dark states known from single-particle quantum optics.

We thank C. Georges, J. Klinder, and L. Broers for helpful discussions. This work was funded by the UP System Balik PhD Program (OVPAA-BPhD-2021-04), the QuantERA II Programme that has received funding from the European Union's Horizon 2020 research and innovation programme under Grant Agreement No. 101017733, the Deutsche Forschungsgemeinschaft (DFG, German Research Foundation) "SFB-925" Project No. 170620586, and the Cluster of Excellence "Advanced Imaging of Matter" (EXC 2056), Project No. 390715994. J. S. acknowledges support from the German Academic Scholarship Foundation.

[*] These authors contributed equally to this work.

[1] K. Baumann, C. Guerlin, F. Brennecke, and T. Esslinger, Dicke quantum phase transition with a superfluid gas in an optical cavity, Nature (London) **464**, 1301 (2010).

[2] H. Ritsch, P. Domokos, F. Brennecke, and T. Esslinger, Cold atoms in cavity-generated dynamical optical potentials, Rev. Mod. Phys. **85**, 553 (2013).

[3] J. Klinder, H. Keßler, M. Wolke, L. Mathey, and A. Hemmerich, Dynamical phase transition in the open Dicke model, Proc. Natl. Acad. Sci. U.S.A. **112**, 3290 (2015).

[4] V. D. Vaidya, Y. Guo, R. M. Kroeze, K. E. Ballantine, A. J. Kollár, J. Keeling, and B. L. Lev, Tunable-Range, Photon-Mediated Atomic Interactions in Multimode Cavity QED, Phys. Rev. X **8**, 011002 (2018).

[5] R. H. Dicke, Coherence in spontaneous radiation processes, Phys. Rev. **93**, 99 (1954).

[6] P. Kirton, M. M. Roses, J. Keeling, and E. G. Dalla Torre, Introduction to the Dicke model: From equilibrium to nonequilibrium, and vice versa, Adv. Quantum Technol. **2**, 1800043 (2019).

[7] F. Damanet, A. J. Daley, and J. Keeling, Atom-only descriptions of the driven-dissipative Dicke model, Phys. Rev. A **99**, 033845 (2019).

[8] C. C. Sung and C. M. Bowden, Phase transition in the multimode two- and three-level Dicke model (Green's function method), J. Phys. A **12**, 2273 (1979).

[9] M. Hayn, C. Emary, and T. Brandes, Phase transitions and dark-state physics in two-color superradiance, Phys. Rev. A **84**, 053856 (2011).

[10] V. M. Bastidas, C. Emary, B. Regler, and T. Brandes, Nonequilibrium Quantum Phase Transitions in the Dicke Model, Phys. Rev. Lett. **108**, 043003 (2012).

[11] R. Chitra and O. Zilberberg, Dynamical many-body phases of the parametrically driven, dissipative Dicke model, Phys. Rev. A **92**, 023815 (2015).

[12] Z. Zhiqiang, C. H. Lee, R. Kumar, K. J. Arnold, S. J. Masson, A. S. Parkins, and M. D. Barrett, Nonequilibrium phase transition in a spin-1 Dicke model, Optica **4**, 424 (2017).

[13] M. Soriente, T. Donner, R. Chitra, and O. Zilberberg, Dissipation-Induced Anomalous Multicritical Phenomena, Phys. Rev. Lett. **120**, 183603 (2018).

[14] E. I. Rodriguez Chiacchio and A. Nunnenkamp, Dissipation-Induced Instabilities of a Spinor Bose-Einstein Condensate Inside an Optical Cavity, Phys. Rev. Lett. **122**, 193605 (2019).

[15] B. Buča and D. Jaksch, Dissipation Induced Nonstationarity in a Quantum Gas, Phys. Rev. Lett. **123**, 260401 (2019).

[16] K. C. Stitely, S. J. Masson, A. Giraldo, B. Krauskopf, and S. Parkins, Superradiant switching, quantum hysteresis, and oscillations in a generalized Dicke model, Phys. Rev. A **102**, 063702 (2020).

[17] J. Skulte, P. Kongkhambut, H. Keßler, A. Hemmerich, L. Mathey, and J. G. Cosme, Parametrically driven dissipative three-level Dicke model, Phys. Rev. A **104**, 063705 (2021).

[18] L. Broers and L. Mathey, Floquet engineering of non-equilibrium superradiance, SciPost Phys. **14**, 018 (2023).

[19] P. Kongkhambut, H. Keßler, J. Skulte, L. Mathey, J. G. Cosme, and A. Hemmerich, Realization of a Periodically Driven Open Three-Level Dicke Model, Phys. Rev. Lett. **127**, 253601 (2021).

[20] R. Lin, R. Rosa-Medina, F. Ferri, F. Finger, K. Kroeger, T. Donner, T. Esslinger, and R. Chitra, Dissipation-Engineered Family of Nearly Dark States in Many-Body Cavity-Atom Systems, Phys. Rev. Lett. **128**, 153601 (2022).

[21] H. Habibian, A. Winter, S. Paganelli, H. Rieger, and G. Morigi, Bose-Glass Phases of Ultracold Atoms due to Cavity Backaction, Phys. Rev. Lett. **110**, 075304 (2013).
[22] C. Kollath, A. Sheikhan, S. Wolff, and F. Brennecke, Ultracold Fermions in a Cavity-Induced Artificial Magnetic Field, Phys. Rev. Lett. **116**, 060401 (2016).
[23] F. Mivehvar, F. Piazza, and H. Ritsch, Disorder-Driven Density and Spin Self-Ordering of a Bose-Einstein Condensate in a Cavity, Phys. Rev. Lett. **119**, 063602 (2017).
[24] C. Georges, J. G. Cosme, L. Mathey, and A. Hemmerich, Light-Induced Coherence in an Atom-Cavity System, Phys. Rev. Lett. **121**, 220405 (2018).
[25] M. Landini, N. Dogra, K. Kroeger, L. Hruby, T. Donner, and T. Esslinger, Formation of a Spin Texture in a Quantum Gas Coupled to a Cavity, Phys. Rev. Lett. **120**, 223602 (2018).
[26] J. G. Cosme, J. Skulte, and L. Mathey, Time crystals in a shaken atom-cavity system, Phys. Rev. A **100**, 053615 (2019).
[27] N. Dogra, M. Landini, K. Kroeger, L. Hruby, T. Donner, and T. Esslinger, Dissipation-induced structural instability and chiral dynamics in a quantum gas, Science **366**, 1496 (2019).
[28] G. Bentsen, I.-D. Potirniche, V. B. Bulchandani, T. Scaffidi, X. Cao, X.-L. Qi, M. Schleier-Smith, and E. Altman, Integrable and Chaotic Dynamics of Spins Coupled to an Optical Cavity, Phys. Rev. X **9**, 041011 (2019).
[29] S. B. Jäger, M. J. Holland, and G. Morigi, Superradiant optomechanical phases of cold atomic gases in optical resonators, Phys. Rev. A **101**, 023616 (2020).
[30] H. Keßler, P. Kongkhambut, C. Georges, L. Mathey, J. G. Cosme, and A. Hemmerich, Observation of a Dissipative Time Crystal, Phys. Rev. Lett. **127**, 043602 (2021).
[31] C. Georges, J. G. Cosme, H. Keßler, L. Mathey, and A. Hemmerich, Dynamical density wave order in an atom–cavity system, New J. Phys. **23**, 023003 (2021).
[32] R. Rosa-Medina, F. Ferri, F. Finger, N. Dogra, K. Kroeger, R. Lin, R. Chitra, T. Donner, and T. Esslinger, Observing Dynamical Currents in a Non-Hermitian Momentum Lattice, Phys. Rev. Lett. **128**, 143602 (2022).
[33] P. Kongkhambut, J. Skulte, L. Mathey, J. G. Cosme, A. Hemmerich, and H. Keßler, Observation of a continuous time crystal, Science **377**, 670 (2022).
[34] D. Dreon, A. Baumgärtner, X. Li, S. Hertlein, T. Esslinger, and T. Donner, Self-oscillating pump in a topological dissipative atom-cavity system, Nature (London) **608**, 494 (2022).
[35] Z. Zhang, D. Dreon, T. Esslinger, D. Jaksch, B. Buca, and T. Donner, Tunable non-equilibrium phase transitions between spatial and temporal order through dissipation, arXiv: 2205.01461.
[36] M. O. Scully and M. S. Zubairy, *Quantum Optics* (Cambridge University Press, Cambridge, England, 1997).
[37] U. Gaubatz, P. Rudecki, S. Schiemann, and K. Bergmann, Population transfer between molecular vibrational levels by stimulated Raman scattering with partially overlapping laser fields. A new concept and experimental results, J. Chem. Phys. **92**, 5363 (1990).
[38] N. V. Vitanov, A. Rangelov, B. W. Shore, and K. Bergmann, Stimulated Raman adiabatic passage in physics, chemistry, and beyond, Rev. Mod. Phys. **89**, 015006 (2017).
[39] M. Fleischhauer, A. Imamoglu, and J. P. Marangos, Electromagnetically induced transparency: Optics in coherent media, Rev. Mod. Phys. **77**, 633 (2005).
[40] K.-J. Boller, A. Imamoğlu, and S. E. Harris, Observation of Electromagnetically Induced Transparency, Phys. Rev. Lett. **66**, 2593 (1991).
[41] M. O. Scully, S.-Y. Zhu, and A. Gavrielides, Degenerate Quantum-Beat Laser: Lasing without Inversion and Inversion without Lasing, Phys. Rev. Lett. **62**, 2813 (1989).
[42] J. Mompart and R. Corbalán, Lasing without inversion, J. Opt. B **2**, R7 (2000).
[43] E. G. Dalla Torre, J. Otterbach, E. Demler, V. Vuletic, and M. D. Lukin, Dissipative Preparation of Spin Squeezed Atomic Ensembles in a Steady State, Phys. Rev. Lett. **110**, 120402 (2013).
[44] A. Piñeiro Orioli, J. K. Thompson, and A. M. Rey, Emergent Dark States from Superradiant Dynamics in Multilevel Atoms in a Cavity, Phys. Rev. X **12**, 011054 (2022).
[45] See Supplemental Material at http://link.aps.org/supplemental/10.1103/PhysRevLett.130.163603 for more details, which includes Refs. [46,47].
[46] M. Abramowitz and I. A. Stegun, *Handbook of Mathematical Functions with Formulas, Graphs, and Mathematical Tables* (Dover, New York, 1964).
[47] J. Keeling, M. J. Bhaseen, and B. D. Simons, Collective Dynamics of Bose-Einstein Condensates in Optical Cavities, Phys. Rev. Lett. **105**, 043001 (2010).
[48] H. Keßler, J. Klinder, M. Wolke, and A. Hemmerich, Optomechanical atom-cavity interaction in the sub-recoil regime, New J. Phys. **16**, 053008 (2014).
[49] J. Klinder, H. Keßler, C. Georges, J. Vargas, and A. Hemmerich, Bose–Einstein condensates in an optical cavity with sub-recoil bandwidth, Appl. Phys. B **122**, 299 (2016).
[50] A. Polkovnikov, Phase space representation of quantum dynamics, Ann. Phys. (Amsterdam) **325**, 1790 (2010).
[51] H. Keßler, J. G. Cosme, M. Hemmerling, L. Mathey, and A. Hemmerich, Emergent limit cycles and time crystal dynamics in an atom-cavity system, Phys. Rev. A **99**, 053605 (2019).
[52] Richelle Jade L. Tuquero, J. Skulte, L. Mathey, and J. G. Cosme, Dissipative time crystal in an atom-cavity system: Influence of trap and competing interactions, Phys. Rev. A **105**, 043311 (2022).
[53] O. Penrose and L. Onsager, Bose-Einstein condensation and liquid helium, Phys. Rev. **104**, 576 (1956).
[54] A. U. J. Lode and C. Bruder, Fragmented Superradiance of a Bose-Einstein Condensate in an Optical Cavity, Phys. Rev. Lett. **118**, 013603 (2017).